Kinetic Signature of Cooperativity in the Irreversible Collapse of a Polymer

Vittore F Scolari, Guillaume Mercy, Romain Koszul, Annick Lesne, Julien Mozziconacci

▶ **To cite this version:**

Vittore F Scolari, Guillaume Mercy, Romain Koszul, Annick Lesne, Julien Mozziconacci. Kinetic Signature of Cooperativity in the Irreversible Collapse of a Polymer. Physical Review Letters, 2018, 121 (5), pp.057801. 10.1103/PhysRevLett.121.057801 . hal-01992814

HAL Id: hal-01992814

https://hal.sorbonne-universite.fr/hal-01992814

Submitted on 24 Jan 2019

HAL is a multi-disciplinary open access archive for the deposit and dissemination of scientific research documents, whether they are published or not. The documents may come from teaching and research institutions in France or abroad, or from public or private research centers.

L'archive ouverte pluridisciplinaire **HAL**, est destinée au dépôt et à la diffusion de documents scientifiques de niveau recherche, publiés ou non, émanant des établissements d'enseignement et de recherche français ou étrangers, des laboratoires publics ou privés.

Distributed under a Creative Commons Attribution 4.0 International License

Kinetic signature of cooperativity in the irreversible collapse of a polymer

Vittore F. Scolari,[1,2,*] Guillaume Mercy,[1,2] Romain Koszul,[1,2] Annick Lesne,[3,†] and Julien Mozziconacci[3,‡]

[1] *Spatial Regulation of Genomes, Genomes & Genetics Department, Institut Pasteur, Paris, 75015, France*
[2] *UMR3525, Centre National de la Recherche Scientifique, Paris, 75015, France*
[3] *Sorbonne Université, CNRS, Laboratoire de Physique Théorique de la Matière Condensée, LPTMC, F-75252 Paris, France*

(Dated: April 10, 2018)

We investigate the kinetics of a polymer collapse due to the formation of irreversible crosslinks between its monomers. Using the contact probability $P(s)$ as a scale-dependent order parameter depending on the chemical distance s, our simulations show the emergence of a cooperative pearling instability. Namely, the polymer undergoes a sharp conformational transition to a set of absorbing states characterized by a length scale ξ corresponding to the mean pearl size. This length and the transition time depend on the polymer equilibrium dynamics and the crosslinking rate. We confirm experimentally this transition using a DNA conformation capture experiment in yeast.

The collapse dynamic of a polymer chain has motivated multiple theoretical and experimental investigations [1–10]. The seminal work of de Gennes, considering a collapse caused by solvent quality reduction with no effects of topological constraints, predicted a continuous conformational transition through successive crumpling stages commonly called the "expanding sausage model" [1]. Grosberg *et al.* proposed a two-stage model, where a fast collapse is followed by a slow unknotting of topological constraints through reptation [2]. The meta-stable intermediate state, called "fractal-globule", preserves the fractal features of a coil while being compact as a globule. The predicted existence of meta-stability was experimentally confirmed by Chu *et al.* [3]. The stability of the fractal globule has been further investigated in theoretical studies which quantified the relaxation of this state towards an equilibrium globule. [11, 12] As another description of polymer collapse, Buguin *et al.* introduced the concept of pearling through the existence of a characteristic size, there explained by nucleation theory [4]. Pearling has been subsequently studied in different works [5–8, 10]. More recently Bunin and Kardar proposed an effective model of polymer collapse, consisting in a cascading succession of coalescence events of blobs actively compressed in a central potential [9].

All these studies investigate the collapse of a polymer under a deep quench: i.e. starting from a equilibrium conformation, interactions between all the monomers or between the monomers and an external potential are abruptly changed and the system relaxes to a new equilibrium state. All the memory about the collapse process is lost in this final state. In contrast, we here study the collapse dynamics of a chain when it is caused by the cumulative effect of irreversible cross-links between monomers. In this case, cross-links cannot be undone and the final state depends on the collapse dynamics. This process has important applications in material science (e.g. vulcanization) and in molecular biology (e.g. cell fixation)

In order to describe the system, we consider here a scale-dependent order parameter: the contact probability curve $P_t(s)$, defined as the mean number of crosslinks present at time t between two monomers at a chemical distance s. This order parameter has two important advantages: it reflects the appearance of local structures such as pearls, and it is a direct observable in the chromosome conformation capture experiments described at the end of this letter.

We first describe the *in silico* dynamics. We run a rejection kinetic Monte Carlo simulation [13, 14] reproducing the Rouse phenomenology on 2048 beads connected initially by a linear chain of links of maximum length b. Each time two non-linked beads come in close vicinity (i.e. their distance fall less then $r_{int} = b/64$), a new link is made with a probability p reflecting the crosslinking rate (details in Supplementary materials (SM) §I.A). These links are then treated exactly as the links between consecutive monomers in the chain.

In the absence of crosslinking, the correlations of bead positions along time and along the chain satisfy the Rouse scaling relations with coefficients C_t and C_s [15]:

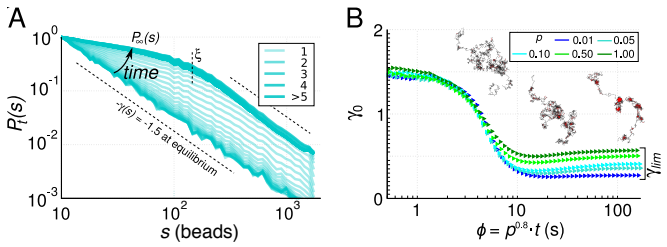

FIG. 1. Kinetics of the pearling transition (simulation). (A) Time evolution of the contact probability curve $P_t(s)$ at fixed crosslink probability $p = 0.1$, displayed as a superposition of semitransparent plots obtained at increasing simulation time t (black arrow); the resulting color density is given in the inset. A crossover at a length ξ arises at large enough times. Error bars are smaller than the thickness of the line. (B) Evolution of γ_0, the short-distance slope of the log-log plot of the $P_t(s)$, as a function of the rescaled time variable ϕ, for different values of p. Inset: snapshots of the time evolution of the polymer conformation ($p = 0.1$).

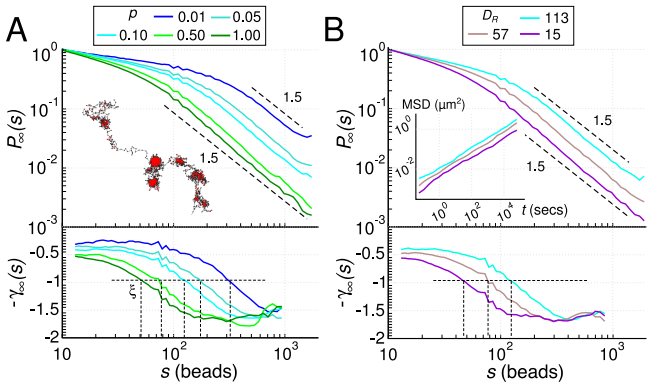

FIG. 2. Quantitative features of the pearling transition (simulation). (A) (Upper panel) asymptotic curve $P_\infty(s)$ and (Lower panel) its local slope $\gamma_\infty(s)$ and pearling length ξ, for different crosslink probabilities p. Inset: example of a pearled state ($p = 0.1$). (B) (Upper panel) asymptotic curve $P_\infty(s)$ and (Lower panel) its local slope $\gamma_\infty(s)$ for different polymer dynamics, parameterized by the Rouse coefficient D_R. Inset: monomer mean square displacement (MSD) as a function of time, whose intercept yields a measurement of C_t, see Eq. 1.

$$\left\langle \left| \vec{R}(0,t_0) - \vec{R}(0,t+t_0) \right|^2 \right\rangle \sim C_t \cdot t^{1/2},$$
$$\left\langle \left| \vec{R}(s_0,0) - \vec{R}(s+s_0,0) \right|^2 \right\rangle \sim C_s \cdot s. \quad (1)$$

After thermal equilibration of the chain, crosslinking is introduced as a succession of irreversible and configuration-dependent changes in the chain topology. As a proxy for steric constraints, we limit the crosslink events to a maximum number per bead, N_{max}, known as the monomer functionality, and stop the simulation once this number is reached for all the beads. N_{max} is equal to 4 in figures if not otherwise specified.

Given this dynamics, the contact probability $P_t(s; p, C_s, C_t)$ is a function of s, the crosslink probability p, the Rouse coefficients and the elapsed time t from the crosslinking onset. At constant p, the time evolution of this curve displays a transition from the equilibrium contact probability, scaling as $\propto s^{-\gamma}$ with $\gamma = 3/2$, [16], to an asymptotic shape $P_\infty(s)$ displaying a crossover between two different scaling behaviors at short and long chemical distances (fig. 1A). This shape and the crossover length ξ reflect the population average features of the absorbing states reached by the polymer at crosslink saturation. The exponent $\gamma_0(t)$, corresponding to the value at short distances of the local exponent $\gamma(s;t)$ defined from the discrete differential

$$\gamma(s;t) = -\frac{\Delta \ln[P(s;t)]}{\Delta \ln[s]}, \quad (2)$$

presents a sharp decrease in time (fig. 1B, cyan symbols).

We first investigated the effect of the crosslink probability p on the asymptotic curve $P_\infty(s)$ (fig. 2A, upper panel). The crossover length ξ can be estimated as the middle point in the transition of the asymptotic exponent $\gamma_\infty(s)$ from short-distance to large-distance values (fig. 2A, lower panel). This length ξ corresponds to the average length of the polymer segments captured in the pearls, and will hereafter be referred as the pearling length. Individual pearls were identified by clustering together monomers on the contact graph using the Louvain algorithm and their size was computed in order to confirm that ξ indeed reflects the average number of monomers in pearls. (see suppl. fig. 5).

The characteristic length ξ could also be recovered from the mean squared distance between monomers as a function of the chemical distance s. For $s > \xi$, $\gamma_\infty(s) = 3/2$, consistent with the initial equilibrium state of the polymer, whereas $\gamma_\infty(s)$ tends inside the pearls to a limiting value $\gamma_{lim} < 1$ at small enough s.

The length ξ scales with the crosslink probability p as $\xi \propto p^{-\delta}$, with $\delta = 0.4$ (fig. 3A), indicating that the extent along the chain of the crosslink-induced collapse is paradoxically more prominent for small p, i.e. low crosslinking rate. Indeed, conformation changes of polymer loops of size greater than ξ are diffusion-limited, while for smaller loops, Rouse diffusion is faster than the crosslinking reaction. In this latter reaction-limited regime, many conformational fluctuations and contacts can occur and be fixed by crosslinks, producing pearls of mean size ξ. Based on this qualitative picture, we propose a mean-field calculation of the dependence of ξ in p. The relaxation time for a fixed loop of size s scales as:

$$\tau_R(s) = D_R^{-1} \cdot s^2, \quad \text{with} \quad D_R = \frac{\pi^3}{4}\left(\frac{C_t}{C_s}\right)^2, \quad (3)$$

(detailed derivation in SM §II.C.4) while the average duration τ_{cross} needed to crosslink contacting beads is inversely proportional to the crosslink probability:

$$\tau_{cross} \propto p^{-1}. \quad (4)$$

Writing that the pearling length ξ emerges from the competition between these two dynamical processes yields:

$$\xi(p) \propto p^{-\delta}, \quad (5)$$

with $\delta = 1/2$ correctly recapitulating the decrease of ξ at increasing p. We here assumed that the dynamics is consistent with Rouse diffusion during the pearling formation and collapse. However, Rouse diffusion is not expected to apply to the mesh into what the initially linear polymer is transformed after enough crosslinks, which may explain the different value $\delta = 0.4$ measured in the simulations (fig. 3A). With the same argument we also predict that ξ varies with the dynamical properties of the polymer. Simulations actually show that variation of the

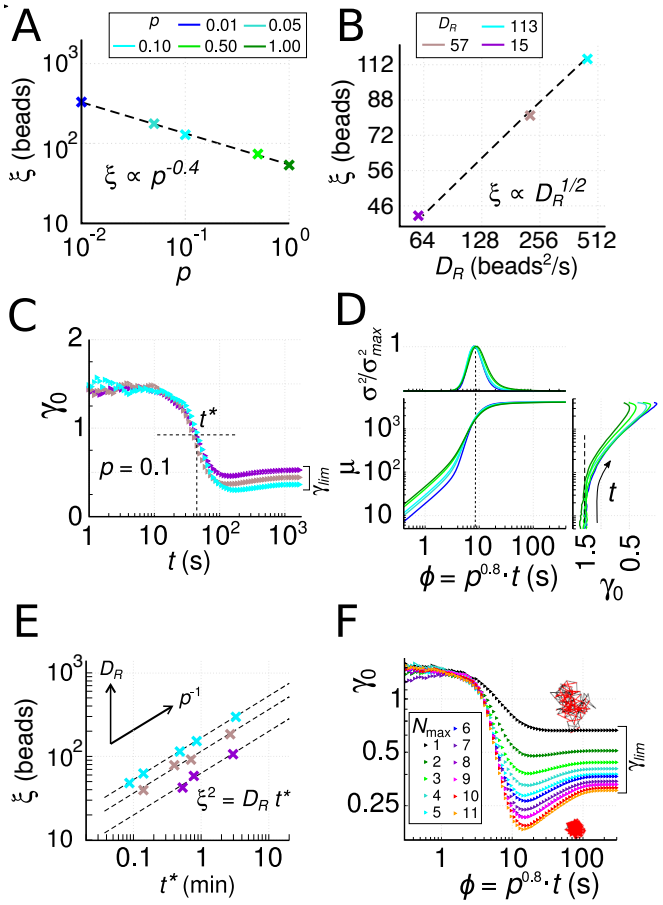

FIG. 3. Dependence of the transition dynamics on the kinetic parameters (simulation) (A) Variation of the pearling length ξ with the crosslink probability p. (B) Variation of the pearling length ξ with the Rouse coefficient D_R. (C) Time evolution of γ_0 at different D_R, Eq. 3 at fixed $p = 0.1$. (D) (Lower panel) Mean cumulative number μ of crosslink events and (Upper panel) its normalized variance σ^2/σ^2_{max} as a function of ϕ, and (Right panel) scatterplot of μ and γ_0. (E) Scatter plot of the pearling length ξ and the transition time t^*; dashed lines are plotted using Eq. 8. (F) Evolution of γ_0 as a function of ϕ for different values of the monomer functionality N_{max}.

Rouse diffusion coefficient D_R has a dramatic effect on ξ (fig. 2B). For small D_R, ξ is small and crosslinking has mostly a local effect. When D_R increases, longer polymer segments can reach their equilibrium conformation between two crosslink events so that ξ becomes larger. In the line of the above calculation, we expect a scaling

$$\xi(D_R) \propto D_R^{1/2}, \tag{6}$$

which is well reproduced in the simulations (fig. 3B).

Our simulation moreover shows that the collapse happens abruptly. The short-distance exponent γ_0 presents a sharp decrease at a time t^*, which we call the pearling time. Before this transition, $t \ll t^*$, γ_0 coincides with the exponent at long distances, 3/2, as expected for an equilibrium state; only after the transition a smaller exponent is observed, with a limiting value $\gamma_{lim} < 1$ depending on the kinetic parameters. t^* depends on the crosslink probability with a scaling $t^* \propto p^{-0.8}$ prompting to define a re-scaled variable $\phi = p^{0.8} \cdot t$. The evolution of γ_0 as a function of ϕ re-scales at any p into a single transition curve (fig. 1B). The scaling of the transition time t^* can also be explained with the above mean-field argument: as t^* emerges from pearling (see polymer snapshots along the transition curve in fig. 1B), it is equal to the relaxation time of pearls of mean size ξ: $t^* = \tau_R(\xi)$. From Eq. 3,

$$t^* \propto p^{-2\delta}, \tag{7}$$

and $\phi^* = p^{2\delta} \cdot t$. As predicted by the above argument and confirmed in the simulation, the transition time does not depend on the Rouse diffusion coefficient D_R (fig. 3C). The pearling transition is the result of the cooperative effect of multiple crosslinks, that takes place only after relaxation of loops with length $s < \xi$. This effect is highlighted in fig. 3D, lower panel, that shows the acceleration of crosslink events at the transition. This process is accompanied by the decrease of γ_0 (3D, right panel) and a large increase of crosslink number variability, due to the fluctuation in the size and time of pearl formation and consistent with a phase transition (3D, upper panel). Collecting the results from simulations performed at various values of crosslink probability p and fixed Rouse diffusion coefficient D_R, the transition points in the plane defined by transition time t^* and pearling length ξ (fig. 3E) satisfy the Rouse scaling relation:

$$t^* = D_R^{-1} \cdot \xi^2; \tag{8}$$

that fully recapitulates the interplay between the pearling time, the pearling length and the polymer dynamics. We finally determine the influence of steric constraints on the final state by changing the monomer functionality N_{max}. While ξ and t^* do not depend on N_{max}, the pearl formation and final internal conformation do, as shown by the time behavior of γ_0. After a transition in t^*, this short-distance exponent transiently goes toward 0 for large enough values of N_{max} before plateauing to an asymptotic value γ_{lim} varying from 0.3 to 0.7 when N_{max} varies (see fig. 3F and suppl. fig. 6). Examination of the conformational trajectories shows that this behavior can be explained by a two-stage dynamics taking place after the transition in t^*. The first stage is the formation of densely connected pearls (in red on the snapshots of fig. 1A) linked by stretched linkers containing fewer monomers. In these pearls, virtually any monomer can contact any other monomer and γ_0 strongly decreases. A slower process then kicks in: the diffusion-limited crumpling of the stretched linkers between adjacent pearls (see the snapshots in fig. 3F). Since in the stretched linkers mostly neighboring monomer are able to come into proximity, the contribution of this collapse to the $p(s)$ is such that γ_0 mildly increases.

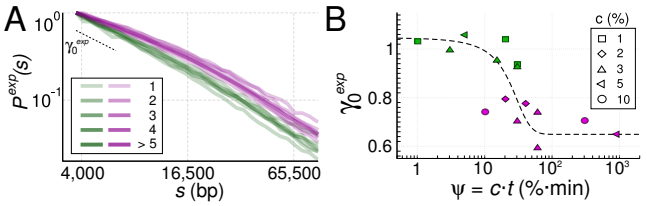

FIG. 4. (A) Experimental contact probability curves $P^{exp}(s)$ for various crosslinker concentrations c, displayed as a superposition of semitransparent plots (see Fig. 1A). (B) Evolution of the experimental slope γ_0^{exp} as a function of the re-scaled time variable $\psi = c \cdot t$ (see fig. 1B). The color discriminates the experiments belonging to the two modalities for γ_0^{exp}, the dashed line is a guide for the eyes.

In summary, our simulation has shown how the interplay between the polymer Rouse dynamics and the rate at which crosslinks are made induces a cooperative phase transition to pearled conformations with characteristic scale ξ. We thus obtained a two-stage pearling kinetics, what has already been described in the literature, however with some significant differences in the underlying mechanisms. In our irreversible model is not compatible with a simple nucleation and growth process: in the nucleation-inspired model of Buguin *et al.* [4] pearls created with a minimal size of ξ grow continuously until the overall polymer collapse. We can also exclude knotting effects: Grosberg *et al.* [2] focused on the role of knots in the conformational relaxation and predicted a dense globule with a fractal dimension of 3 and a relaxation through reptation. In contrast, we neglect volume interactions which are a necessary element for knot stability. In order to see if the appearance of a specific length scale depends on the fact that we used phantom chain, we performed to extra simulation taking explicitly into account steric effect. We found in this case that the pearling dynamics of the transition is unchanged (see suppl. fig. 7). We also recovered the local formation of a crumple globule-like state in each pearls with $\gamma_0 = 1$ The emergence of the characteristic length ξ however excludes the fractality of the absorbing conformations. The scale depend behavior observed in our simulation reflects the presence of two different dynamics: reaction-limited pearling at short distances along the chain, diffusion-limited collapse at large distances.

Experimental approaches in chromosome biology have been recently renewed by chromosome conformation capture (3C) that uses a succession of crosslinking, restriction, religation and sequencing steps to measure contact frequencies along a DNA molecule *in vivo*. This technique centrally exploits the unique opportunity offered by the DNA heteropolymer to have a single sequence identifier at each loci (for long enough identifiers) and so to derive contact probability curves from crosslink counts.

In the seminal paper introducing the genome-wide 3C technique, Hi-C, Lieberman-Aiden *et al.* [17] derived the contact probability curve $P(s)$ from crosslink counts, as a function of the genomic distance s. In the range between 1 and 10 millions base pairs (bp), these authors fitted the resulting curve with a scaling relation $P(s) \propto s^{-\gamma}$, with a value of γ close to 1 compatible with the value expected for the fractal-globule state. However, an exponent of 0.75 has also been reported at shorter scale in two human-cell studies, and other out-of-equilibrium mechanisms were invoked to explain this alternative exponent: the tension globule [18] or the extrusion of loops by molecular motors such as condensins [18–20]. While these models can have important implications on the role of chromosome folding in cells, they do not take explicitly into account the potential distortion that the DNA polymer can undergo during the initial step of the experiment, consisting in chemically crosslinking DNA with formaldehyde. This crosslinking step prompted us to exploit this experimental technique to check the collapse scenario described in our simulations.

In order to start from configurations that are the closest to an simple homopolymer, we used synchronized yeasts that are not replicating nor dividing. We performed Hi-C experiment at different formaldehyde concentrations c and exposure times t in order to observe the evolution of the polymer conformation during the crosslink-induced collapse. Not knowing the reaction order, we cannot establish an exact mapping between k_{on} and c, so we used a simple ansatz, $\psi = c \cdot t$, for the rescaled time variable. The experimental curves $P^{exp}(s)$ cluster around two different mean-curves differing by their slope at short distances γ_0^{exp} (Fig. 4A). When plotting this exponent as a function of ψ, we observe a sharp transition (Fig. 4B) as predicted by the simulations. Two differences are nevertheless worth discussing. Before the transition, the short-distance exponent of yeast chromosomes is not equal to 1.5 as in the simulations (fig. 1B), but to 1 (0.05 *s.d.*). This value might either correspond to an effect of volume interactions during the early phases of pearling collapse or to an *in-vivo* special organization of the DNA in chromosomes, potentially induced by the regular wrapping of DNA around the nucleosomal protein spools. For distances above 10 kb these constraints weaken and the chain follows a more typical random walk with an exponent closer to 1.5. After the transition, γ_0^{exp} is equal to 0.7 (0.06 *s.d.*), corresponding to the value observed for $N_{max} = 1$ in our simulations. This value is likely explained by strong steric constraints preventing a crosslinked locus to contact other loci. The precise estimation of ξ was impaired by the higher biological, experimental and statistical noise on $P(s)$ at increasing distance s so that we could not measure experimentally the dependency of ξ on the crosslinker concentration. Nevertheless, the experiment clearly demonstrate that a polymer experiencing a crosslink-induced collapse undergoes a sudden transition. It also confirms that inside pearls, at length scales lower than ξ, the polymer conformation in

the absorbing asymptotic state is very compact, with an exponent γ_0 lower than 1, whereas the polymer topology remains unchanged at longer length scales.

We thanks Madan Rao, John Marko, Jean-Marc Victor, Benjamin Audit, Marco Cosentino-Lagomarsino, Maxim Dolgushev and Daniel Jost for the extremely useful discussions and suggestions, and Véronique Legrand and the DSI of Institut Pasteur for the computational power and assistance.

* vittore.scolari@gmail.com
† Second affiliation: IGMM, University of Montpellier, CNRS, Montpellier, France
‡ mozziconacci@lptmc.jussieu.fr

[1] P. De Gennes, Journal de Physique Lettres **46**, 639 (1985).
[2] A. Y. Grosberg, S. K. Nechaev, and E. I. Shakhnovich, Journal de physique **49**, 2095 (1988).
[3] B. Chu, Q. Ying, and A. Y. Grosberg, Macromolecules **28**, 180 (1995).
[4] A. Buguin, F. Brochard-Wyart, and P. De Gennnes, Comptes rendus de l'Académie des sciences. Série II, Mécanique, physique, chimie, astronomie **322**, 741 (1996).
[5] B. Ostrovsky, G. Crooks, M. Smith, and Y. Bar-Yam, Parallel Computing **27**, 613 (2001).
[6] E. Pitard and J.-P. Bouchaud, The European Physical Journal E: Soft Matter and Biological Physics **5**, 133 (2001).
[7] N. V. Dokholyan, E. Pitard, S. V. Buldyrev, and H. E. Stanley, Physical Review E **65**, 030801 (2002).
[8] A. Halperin and P. M. Goldbart, Physical Review E **61**, 565 (2000).
[9] G. Bunin and M. Kardar, Physical review letters **115**, 088303 (2015).
[10] S. Majumder, J. Zierenberg, and W. Janke, Soft matter **13**, 1276 (2017).
[11] R. D. Schram, G. T. Barkema, and H. Schiessel, The Journal of chemical physics **138**, 224901 (2013).
[12] A. Chertovich and P. Kos, The Journal of chemical physics **141**, 134903 (2014).
[13] A. Cacciuto and E. Luijten, Nano Letters **6**, 901 (2006).
[14] V. F. Scolari and M. C. Lagomarsino, Soft matter **11**, 1677 (2015).
[15] M. Doi and S. F. Edwards, *The theory of polymer dynamics*, Vol. 73 (oxford university press, 1988).
[16] P.-G. De Gennes, *Scaling concepts in polymer physics* (AIP, 1980).
[17] E. Lieberman-Aiden, N. L. Van Berkum, L. Williams, M. Imakaev, T. Ragoczy, A. Telling, I. Amit, B. R. Lajoie, P. J. Sabo, M. O. Dorschner, *et al.*, Science **326**, 289 (2009).
[18] A. L. Sanborn, S. S. Rao, S.-C. Huang, N. C. Durand, M. H. Huntley, A. I. Jewett, I. D. Bochkov, D. Chinnappan, A. Cutkosky, J. Li, *et al.*, Proceedings of the National Academy of Sciences **112**, E6456 (2015).
[19] G. Fudenberg, M. Imakaev, C. Lu, A. Goloborodko, N. Abdennur, and L. A. Mirny, Cell reports **15**, 2038 (2016).
[20] T. Terakawa, S. Bisht, J. M. Eeftens, C. Dekker, C. H. Haering, and E. C. Greene, Science **358**, 672 (2017).